Magnetic Resonance Imaging 61 (2019) 285–295

Contents lists available at ScienceDirect

Magnetic Resonance Imaging

journal homepage: www.elsevier.com/locate/mri

Original contribution

Improved gray matter surface based spatial statistics in neuroimaging studies

Prasanna Parvathaneni[a,*], Ilwoo Lyu[b], Yuankai Huo[a], Baxter P. Rogers[c], Kurt G. Schilling[c], Vishwesh Nath[b], Justin A. Blaber[a], Allison E. Hainline[d], Adam W. Anderson[c], Neil D. Woodward[e], Bennett A. Landman[a,b,c,e]

[a] Electrical Engineering, Vanderbilt University, Nashville, TN, USA
[b] Computer Science, Vanderbilt University, Nashville, TN, USA
[c] Vanderbilt University Institute of Imaging Science, Vanderbilt University, Nashville, TN, USA
[d] Biostatistics, Vanderbilt University, Nashville, TN, USA
[e] Department of Psychiatry and Behavioral Sciences, Vanderbilt University, Nashville, TN, USA

ARTICLE INFO

Keywords:
NODDI
AMICO
Microstructure imaging
Spatial statistics
Gray matter
Advanced DW-MRI
Functional MRI
GBSS
TBSS
GS-BSS
Ciftify

ABSTRACT

Neuroimaging often involves acquiring high-resolution anatomical images along with other low-resolution image modalities, like diffusion and functional magnetic resonance imaging. Performing gray matter statistics with low-resolution image modalities is a challenge due to registration artifacts and partial volume effects. Gray matter surface based spatial statistics (GS-BSS) has been shown to provide higher sensitivity using gray matter surfaces compared to that of skeletonization approach of gray matter based spatial statistics which is adapted from tract based spatial statistics in diffusion studies. In this study, we improve upon GS-BSS incorporating neurite orientation dispersion and density imaging (NODDI) based search (denoted N-GSBSS) by 1) enhancing metrics mapping from native space, 2) incorporating maximum orientation dispersion index (ODI) search along surface normal, and 3) proposing applicability to other modalities, such as functional MRI (fMRI). We evaluated the performance of N-GSBSS against three baseline pipelines: volume-based registration, FreeSurfer's surface registration and ciftify pipeline for fMRI and simulation studies. First, qualitative mean ODI results are shown for N-GSBSS with and without NODDI based search in comparison with ciftify pipeline. Second, we conducted one-sample *t*-tests on working memory activations in fMRI to show that the proposed method can aid in the analysis of low resolution fMRI data. Finally we performed a sensitivity test in a simulation study by varying percentage change of intensity values within a region of interest in gray matter probability maps. N-GSBSS showed higher sensitivity in the simulation test compared to the other methods capturing difference between the groups starting at 10% change in the intensity values. The computational time of N-GSBSS is 68 times faster than that of traditional surface-based or 86 times faster than that of ciftify pipeline analysis.

1. Introduction

Gray matter (GM) in the cerebral cortex is key to many sensory, cognitive, and motor functions of the brain. Detecting cortical alterations with neuropathologic conditions could provide potential biomarkers to facilitate early diagnosis and assessment of disease severity. In recent years, the development of neuroimaging techniques, such as high-resolution magnetic resonance imaging (MRI), functional magnetic resonance imaging (fMRI), diffusion weighted magnetic resonance imaging (dMRI), positron emission tomography (PET) or single photon emission computed tomography (SPECT), have promoted the identification of structural and functional characteristics of the developing brain and underlying mental disorders [1–7]. An increasing number of studies have shown structural and functional gray matter changes in clinical applications - e.g., amyotrophic lateral sclerosis [8], schizophrenia and bipolar disorder [9,10], age related effects [11], attention deficit hyperactivity disorder [12], and Alzheimer's disease [13]. While T1 images can be acquired at high resolution (e.g., 1 mm isototropic), clinical imaging in other modalities (such as dMRI and fMRI) are constrained by imaging and physiological factors leading to lower resolution (2–3 mm isotropic). As the cortex is about 1.6–4.5 mm thick [14–16] within the gray matter tissue region between white and

* Corresponding author.
E-mail address: Prasanna.Parvathaneni@Vanderbilt.edu (P. Parvathaneni).

https://doi.org/10.1016/j.mri.2019.05.016
Received 2 March 2019; Received in revised form 7 May 2019; Accepted 9 May 2019

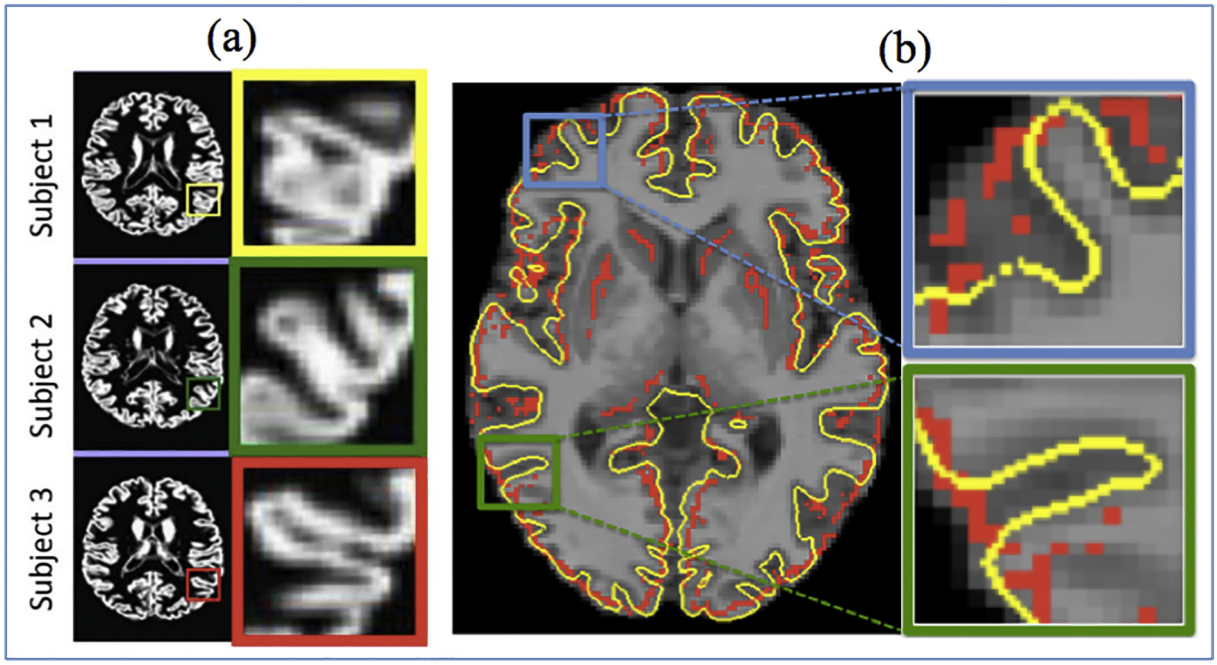

Fig. 1. (a) Non-rigid image registration of GM probability maps of three subjects. Each color box highlights the corresponding region of interest. Right column shows detailed differences in cortical folding patterns across the subjects. (b) Skeletonized GM (red) and cortical central surface (yellow) are overlaid on T1 image. GM central surface closely follows the cortical structure compared to that of skeletonized GM approach. Two examples are highlighted in blue and green boxes where GM cortical surface closely follows the cortical structure compared to the volumetric based GM skeletonization approach. Darker regions on T1 indicate GM and lighter regions represent WM. (For interpretation of the references to color in this figure legend, the reader is referred to the web version of this article.)

pial surfaces, significant challenges arise with cross subject analysis involving registration artifacts and partial volume effects [17]. The individual cortical anatomy may not be sufficiently aligned after non-rigid volumetric registration since it is quite challenging to incorporate spatial coherence in the volumetric images (see Fig. 1-a). In particular, volumetric smoothing potentially introduces partial volume effects since the cortical structure is thinner, as seen in Fig. 1-b. This issue was successfully addressed in WM using tract based spatial statistics (TBSS) [18], which has proven to be a popular technique for performing voxel-wise statistical analysis with improved sensitivity and interpretability of analysis of multi-subject diffusion imaging studies in white matter (WM) [19–23]. Gray matter based spatial statistics (GBSS) adapted the TBSS framework for GM using neurite orientation dispersion and density imaging (NODDI) [11] to perform voxel-wise statistical analysis on GM microstructure in diffusion studies. GBSS employs skeletonized cortical ribbon to capture diffusion metrics along its trajectories. However, this approach could yield low sensitivity to the cross sectional differences around the cortical sulci since GM skeletonization is extracted only along highly overlapping regions. To overcome this issue, we proposed an alternate approach known as gray matter surface based spatial statistics (GS-BSS) [24] that employs a cortical surface to increase the number of highly probable GM vertices that closely follow the cortex (Fig. 1b).

In volumetric neuroimaging analyses, spatial smoothing is generally performed to improve image alignment and statistical sensitivity, at the cost of specificity of the underlying region of interest [25]. As the GM of healthy adult subjects is typically < 5 mm thick, spatial smoothing needs to be carefully performed to retain the sensitivity and specificity of the underlying changes [26,27]. Surface-based approaches have been proposed with improved sensitivity in cortical morphometry [25,28–33] over volumetric neuroimaging in both fMRI and cortical features of interest. There is wide agreement that the surface-based morphometric (SBM) analyses [34–36] have theoretical and empirical advantages over traditional voxel-based morphometry (VBM) approaches for addressing the problem of inference in group studies. However, substantial inter-subject variation in the shapes of local features (e.g., mean curvature) still hampers accurate cortical surface registration.

A majority of studies focus on volume- or surface-based analysis on a particular modality [11,37,38]. Few studies [32,38–40] have incorporated multi-modalities into a single integrated pipeline of surface-based analyses. The desire to better understand structural-functional relationships drives the need for robust analysis frameworks. The Human Connectome Project (HCP) minimal preprocessing pipeline [38] is one such approach that integrates multimodal data for cross subject analysis. It is built upon the FreeSurfer software tool (https://surfer.nmr.mgh.harvard.edu) for surface generation and alignment to standard space in addition to defining Connectivity Informatics Technology Initiative (CIFTI) format and grayordinate system that incorporates cortical and subcortical information. In a recent study, multimodal surface matching (MSM) [41] registration is incorporated into a pipeline that uses multimodal registration features containing myelin maps [59], resting-state networks (RSNs) and visuotopic features to drive alignment to a group template. In the HCP approach [38], the data acquisition protocol is customized and often requires newly developed preprocessing methods unlike conventional data acquisition schemes.

There is huge amount of clinical data that is already acquired from healthy individuals and also in different clinical populations that is not acquired as per the HCP proposed standards. Having tools that could provide HCP-style analyses to leverage the existing data to the extent possible will be beneficial for clinical research. The ciftify pipeline [42] bridges the gap for making HCP-style analysis applicable to non-HCP (i.e., legacy) datasets by adapting the key modules from HCP pipeline into existing structural workflows. For functional/diffusion MRI data, the alignment with anatomical T1 plays an important role to map volume data onto the surface. Thus, preprocessing choices need to be made to maximize the data quality given its limitations in legacy datasets. The ciftify pipeline takes the preprocessed data from other modalities and converts it into needed grayordinate format for further analysis.

In this paper, we propose N-GSBSS for carrying out localized statistical testing of neuroimaging data across multiple modalities in GM. Unlike the skeletonization approach in GBSS, cortical surfaces reconstructed from high resolution T1 images are employed to facilitate cross-subject analysis. This method provides a bridge between volume and surface registration approaches to achieve cross-subject correspondence of low resolution image data. This method is an extension of our previous work, GS-BSS [24]. While conceptually similar, improvements are made in registration methodology that allow mapping of the metrics of interest in subject space. The key idea in this method is to incorporate normal search from the cortical surface to get metrics from highly probable GM voxels using the orientation dispersion index (ODI) from the NODDI model. ODI is higher in GM compared to that of WM [43], thus searching for higher ODI could help to locate underlying highly probable GM. Toward this end, we show an application to statistical analysis of fMRI data. To test the sensitivity of the approach, a simulation study is performed by varying region of interest (ROI) size and percentage change of intensity values within the ROI. It is presented as a full end-to-end pipeline to perform such spatial statistics in group analysis. We evaluated the performance of N-GSBSS against three baseline pipelines: volume-based registration (VBR), FreeSurfer's surface registration (SBR) and ciftify pipeline for fMRI and simulation studies. The source code for N-GSBSS is made available at https://github.com/MASILab/N-GSBSS/. The computational time of N-GSBSS is 68 times faster than that of traditional SBR or 86 times faster than the ciftify pipeline method [42].

2. Methods

2.1. Background

GS-BSS method was proposed to perform voxel-based statistical analysis of diffusion microstructure features acquired at low resolution on GM surfaces using high-resolution T1 images. Structural images are segmented and normalized to MNI template space using diffeomorphic anatomical registration using exponentiated lie algebra (DARTEL) method [44]. Diffusion metrics of interest are co-registered to structural T1 and transformed to MNI template space using forward deformation. GM surfaces are deformed to MNI template space using inverse transformation obtained from the registration step. Correspondence between cortical surfaces is obtained with diffeomorphic spectral matching DSM [45] and the mapping is applied to the deformed diffusion microstructure data in MNI template space to project onto the target surface for group analysis. GS-BSS is shown to yield better performance compared to that of VBM or the skeletonization approach of GBSS, which is based on alignment invariant skeleton projection. However, there are some methodological limitations that could impact the sensitivity of such analysis. First, the possibility of having any misalignment between diffusion microstructure and structural images after co-registration, could impact the sensitivity of the analysis to be performed on highly probable GM region. Second, the diffusion metrics of interest are projected onto the GM cortical surface in MNI template space that could allow the prospect of including distortions caused in the data from the volume registration step. Finally while the GM surfaces are used for achieving cortical correspondence, all the data is mapped back into voxel-space before performing statistical analysis.

In this paper, the goal is to improve spatial statistics in GM by projecting all the metrics of interest from each modality onto a single target cortical surface and carry out vertex based statistical analysis. Current work addressed the limitations of GS-BSS and provided improvement in the following areas,

- To overcome possible alignment issues from co-registration step and improve intra-subject correspondence, cortical search is proposed that can further improve the sensitivity of the method.
- To minimize distortions and keep the data as close to the raw images that are acquired as possible, metrics of interest are mapped onto the cortical surface in subject space unlike the GS-BSS method where the metrics of interest are mapped from the volume image in MNI space onto the deformed cortical surface in MNI template space.
- To perform spatial statistics on vertices, unlike the voxel based spatial statistics that is performed in GS-BSS.
- To show applicability of the method in additional modalities like fMRI.

2.2. Subjects and neuroimaging data acquisition

Neuroimaging data were collected on 30 healthy subjects (average age = 31.94 (male, n = 18)/35.83 (female, n = 12)) who participated in an on-going study of brain connectivity in neuropsychiatric disorders. The Vanderbilt University Institutional Review Board approved the study and all participants provided written informed consent prior to enrolling in the study. Neuroimaging data were acquired on a 3 T scanner (Achieva, Philips Medical Systems, Best, The Netherlands) equipped with a 32-channel head coil located at the Vanderbilt University Institute of Imaging Sciences. The following neuroimaging data were acquired on each subject: 1) a T1-weighted 3D-TFE anatomical scan (1 mm isotropic resolution, TE = 2 ms, TR = 8.95 ms and TI = 643 ms), 2) up to 6 functional EPI scans (3 mm resolution during which subjects completed an event related spatial working memory task (described below), and 3) a diffusion-weighted imaging scan protocol (2.5 mm isotropic resolution, with a matrix of 96 × 96, 50 slices, TR = 2.65 s, TE = 101 ms, Gmax = 37.5 mT/m) that included two diffusion shells with b-values of 1000 s/mm^2 (24 directions) and 2000 s/mm^2 (60 directions). Two subjects are excluded from the diffusion processing due to motion-related quality issues in diffusion MRI acquisition. HARDI from one subject is marked unusable due to zipper artifact in B0. Second subject is excluded based on quality checking measures due to subject movement (15 mm movement). Cardiac and respiratory gating were not used.

2.3. Preprocessing

2.3.1. T1 anatomical data processing

Each structural scan was segmented into GM, WM, and cerebrospinal fluid (CSF) tissue classes using the VBM8 toolbox (http://dbm.neuro.uni-jena.de/vbm/) from SPM12 (http://www.fil.ion.ucl.ac.uk/spm). Additionally, each voxel of the images was automatically labeled using multi-atlas segmentation [46] according to the BrainCOLOR protocol [47] into 132 brain regions and 1 background that was used as a preprocessing step for MaCRUISE. The white, central and pial cortical surfaces were reconstructed by MaCRUISE [48] using the topology-preserving geometric deformable surface model. The central surfaces were used in further surface-based processing including registration and mapping volume data onto the surfaces.

2.3.2. Diffusion data processing

Diffusion-weighted images (DWI) were preprocessed using EDDY [49] tool from FMRIB Software Library FSL [50] for eddy current correction and subject motion correction. The registration matrix of each DWI was used to measure patient movement, and the gradient table was rotated accordingly. For diffusion data processing, the data from 2 shells were combined into a single DWI file and corresponding b-values and b-vectors were concatenated accordingly. A scheme file was generated using the fsl2scheme command from Camino (http://camino.cs.ucl.ac.uk). A brain mask was created using the FSL brain extraction tool [51].

For NODDI processing, the DWI file, scheme file and mask (generated as described above) were passed to the AMICO package (https://github.com/daducci/AMICO/), which is a fast implementation of NODDI [43] with linear approximation. Single transformation was

derived using b0 image to co-register to structural T1-weighted scan using spatial normalization from SPM12 with 12-parameter affine registration. Corresponding transformation is applied to NOODI-derived maps of intracellular volume fraction, isotropic volume fraction (V_{iso}), and orientation dispersion index (ODI). These ODI and V_{iso} maps from multiple subjects were used in further analysis and validation of N-GSBSS.

2.3.3. Working memory fMRI processing

During the functional EPI scans, subjects completed a slow event-related spatial working memory task. Briefly, on each trial, three filled circles were presented sequentially, one at a time, during a 3-s encoding phase. The encoding phase was followed by a 16 s delay period during which a fixation dot was shown. Following the delay period, a probe (open circle) was presented for 1 s and subjects had to indicate with a button press whether or not the probe matched one of the previously encoded locations. Each trial was followed by a 14 s inter-trial interval. Subjects complete 30 working memory trials and 18 control trials. The working memory and control trials were identical, except for the fact that subjects were asked not to memorize the locations during the cue period of the control trials and pressed both the yes and no button during the probe period. Different colored circles, red and gray, were used to alert subjects to working memory and control trials, respectively. Preprocessing and generation of first-level, subject-specific statistical parametric maps were performed using spatial normalization in SPM12 [52]. Preprocessing included slice timing and motion correction, and co-registration of each subject's functional EPI scans to their anatomical T1-weighted scans. Subject-specific, voxel-wise maps showing relative difference in the BOLD response between working memory and un-modeled baseline for cue, maintenance, and probe conditions were generated by modeling each subject's time series data. Note, the contrast maps for cue, maintenance, and probe conditions were kept in the individual subject-specific space co-registered to T1 prior to being entered into the N-GSBSS pipeline described below.

2.4. N-GSBSS pipeline

The steps involved in carrying out the spatial statistics starting from the preprocessed multi-modal data to transferring all the metrics of interest onto a single target surface are illustrated in this section. The data from the co-registered volume images is projected onto the GM central surface using enclosing voxel approach. Alignment issues after co-registration would introduce partial volume effects or outliers by fetching data from the voxels that may not belong to highly probable GM. In order to overcome this limitation, cortical search is implemented using ODI measure as it has been shown to be higher in GM compared to that of WM [43].

2.4.1. Cortical search using NODDI maps

Diffusion microstructure indices from NODDI including ODI and V_{iso} are used in the cortical search. First ODI is masked with V_{iso} to exclude any voxels with isotropic volume fraction of > 0.5 indicating CSF regions. The surface normal is calculated at each vertex on the central surface. As the T1 was acquired at 1 mm resolution and the cortical thickness is < 5 mm thick, we search the maximum ODI at each vertex along positive and negative normal directions (2 mm at maximum range with an interval of 1 mm). We create a search map by collecting these enclosing voxels that the normal directions point out. The metrics of interest in other modalities are finally transferred onto the central surface via the search map. Fig. 2(a) illustrates this approach and corresponding histogram of masked ODI is shown in Fig. 2(b) before and after search.

2.4.2. Cortical correspondence on the target surface

Cortical surfaces are highly variable, so roughly similar surfaces would be useful for surface registration. As preprocessing volume registration can provide reasonably well-aligned surfaces, structural T1 is non-linearly registered with MNI template using ANTs SyN registration method (52). Corresponding inverse deformation is applied to the surface as the first step. The vertex coordinates of the surface are converted to RAS format before applying "antsApplyTransformsToPoints" from ANTs toolbox. The deformed coordinates are converted back into original format thus transforming the surface from subject space to MNI space (#2 from Fig. 3). However, as shown in Fig. 1(a), the cortical anatomy is not yet well aligned across the subjects after volume deformation. Then, we refine/update the correspondence using surface registration step [45] in the same way as (24), which is expected to establish better correspondence. It provides mapping information of the cortical surface from each subject onto the target surface (#3 from Fig. 3) on which spatial statistics can be performed.

2.4.3. Project metrics of interest on target surface

As cortical anatomical properties such as cortical thickness were derived from the surface, they were already assigned to each vertex. These properties were then projected onto the target surface via the established shape correspondence from step 3. Images from different modalities are co-registered to T1 anatomical images before proceeding with further analysis as shown in step 4. Cortical ODI search is performed by taking in ODI and V_{iso} measures from the NODDI model to get the corresponding map of highly probable GM vertices for co-registered images (step 5 in Fig. 3). Step 6 illustrates the first level analysis carried out on each modality to derive metrics of interest. In the volume images, the metrics of interest were mapped onto the individual GM surface (step 7 in Fig. 3) from the voxel that encloses the corresponding vertex coordinate obtained from the cortical ODI search (step 5 in Fig. 3). Both dMRI based NODDI metrics and fMRI based working memory contrast maps were projected via the vertex coordinates and the mapped properties were then transferred onto a common target surface (Step 8 in Fig. 3). Spatial statistics across the subjects are performed on the target surface by applying 2 mm smoothing kernel for cross subject analysis. We adapted the Gaussian kernel smoothing proposed by [38], where each vertex was weighted based on data from the neighboring vertices and scaled by the vertex area.

2.4.4. Summary highlighting enhancements

A novel ODI search along surface normal for maximum ODI value is used to probe for highly probable GM regions in the co-registered image. Additionally, enhancements that are made to the earlier method [24] are the transfer of metrics of interest on to the GM cortical surface in the individual subject space instead of MNI space, to reduce the error that could occur with volume and surface deformation to the MNI template. While [24] showed the application to diffusion microarchitecture features, this work extends the applications to fMRI data, thus enabling multimodal analysis across structural and functional changes. Group analysis is performed at vertex level on the target surface.

The evaluation of the approach is carried out in the following ways. 1) We compare qualitative mean ODI, a diffusion microstructure feature, for N-GSBSS with and without cortical ODI based search in comparison with ciftify pipeline. 2) We perform non-parametric permutation testing on contrast maps obtained from first level analysis of working memory tasks in fMRI. 3) We perform a simulation study in structural MRI to evaluate sensitivity and specificity of the approach.

2.5. Spatial statistics

Once all the properties from different modalities were projected on the target surface, GM based vertex-wise spatial statistics were calculated using the Permutation Analysis of Linear Models (PALM) [53] package from the FSL software library (FMRIB; *http://www.fmrib.ox.ac.uk/fsl/*) which performs inference through permutation. Significant

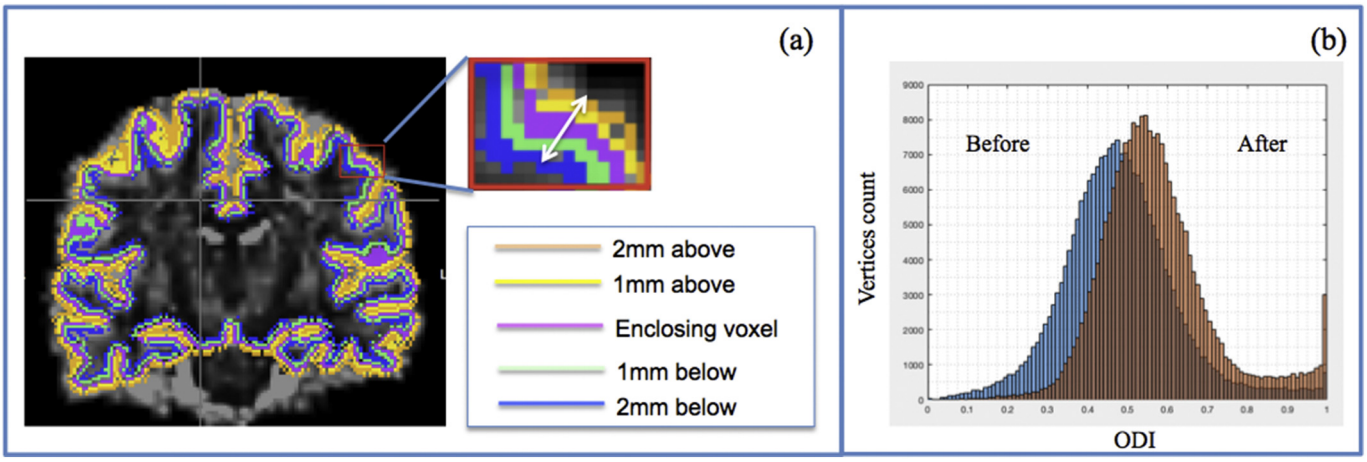

Fig. 2. (a) ODI overlaid with cortical surface mapping based on enclosing voxels, 1 mm above, 2 mm above, 1 mm below and 2 mm below of central surface obtained using normal search. At each vertex, maximum ODI value is selected from these 5 values along the vertex normal (white arrow in zoomed in box) and corresponding map is used for projecting the diffusion metrics on to the cortical surface. (b) Histogram of ODI projected on to the cortical surface on single subject before and after ODI search.

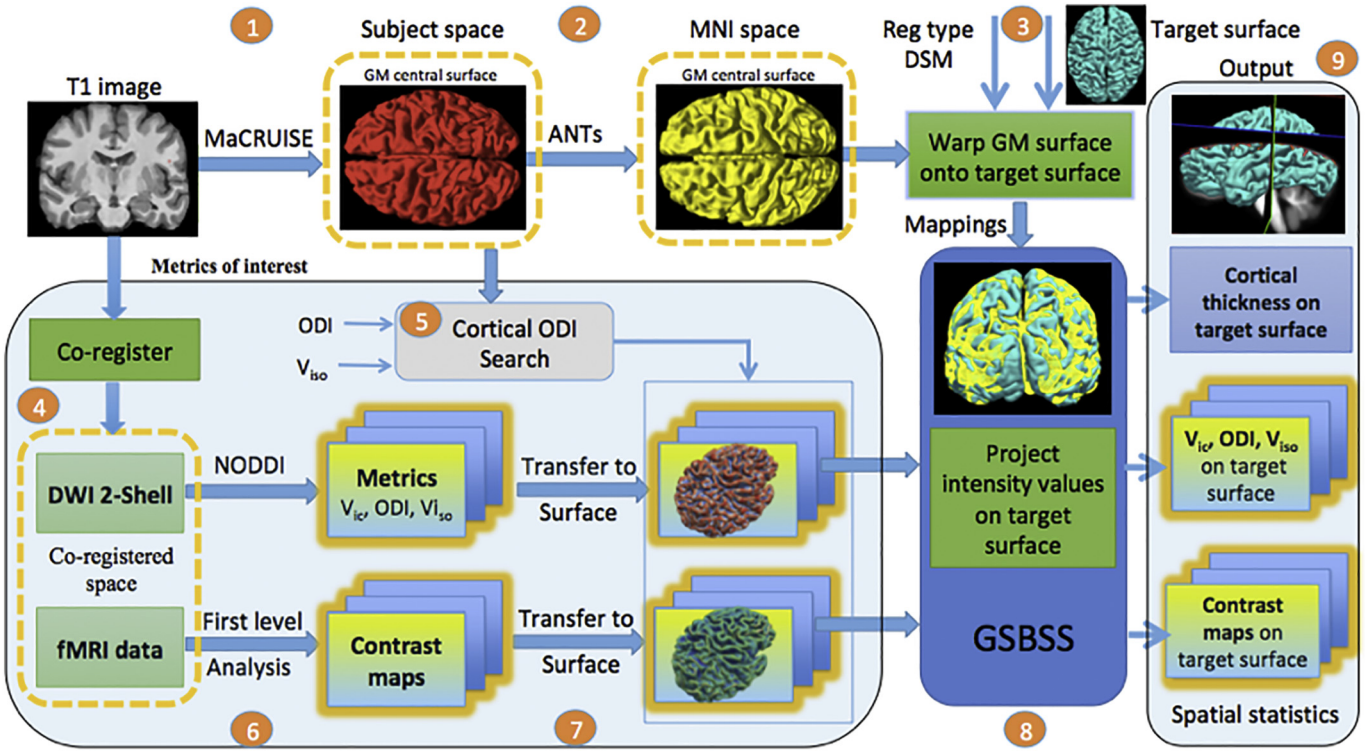

Fig. 3. Flowchart of the N-GSBSS data processing for each subject. (1) The central surface is reconstructed via MaCRUISE (red) (2) and transformed to the MNI space (yellow) using ANTs volume registration. (3) These volumes are diffeomorphically registered to a single target surface. (4) Metrics of interest in other modalities are co-registered to corresponding anatomical T1-weighted image. (5) Cortical ODI search is performed using ODI and V_{iso} from NODDI metrics to search for higher ODI excluding V_{iso} within a given range (6) Data are processed for each modality (NODDI for diffusion microstructure and first level analysis for working memory tasks) to derive metrics of interest for cross-sectional analysis. (7) Metrics of interest are mapped onto the individual surface. (8) The mappings from shape correspondence are used to project intensity values of metrics of interest to the target surface (blue). (9) Vertex-wise spatial statistics on all projected data are performed on the target surface. (For interpretation of the references to color in this figure legend, the reader is referred to the web version of this article.)

results are reported after controlling for family-wise error (FWE) with $p < 0.05$ through threshold free cluster enhancement (TFCE).

2.6. Baseline methods

2.6.1. Volume based registration (VBR) processing

Volume images of metrics of interest from other modalities were registered to MNI template by applying the non-rigid transformation obtained from anatomical T1-weighted images. A GM mask was calculated based on 0.5 thresholds on the GM probability map in each subject and 70% overlap across all the subjects to filter the number of voxels to retain highly probable GM voxels. Gaussian kernel smoothing of 2 mm was applied before performing spatial statistics. Nonparametric permutation based testing was performed on smoothed volume data within a brain mask using FSL PALM [53] (https://fsl.fmrib.ox.ac.uk/fsl/fslwiki/PALM). Statistical results were projected

onto the target surface based on the enclosing voxel approach for visualization and comparison with surface based results.

2.6.2. Surface based registration (SBR) processing

In order to compare the proposed approach, we used the FreeSurfer surface registration method [30] for cortical shape correspondence. Metrics of interest from volume data in subject space were projected onto the central surface using the enclosing voxel approach. These metrics were transferred to the target surface via the shape correspondence and smoothed on the target surface for cross-sectional analysis. In order to make a fair comparison with N-GSBSS results with optimal multiple comparison correction, metrics of interest from two hemispheres were considered as a single dataset before carrying out the permutation based statistical tests.

2.6.3. Ciftify pipeline processing

The ciftify pipeline [42] has been developed to facilitate grayordinate-based analysis in CIFTI format for legacy datasets. In preprocessing, surface reconstruction is carried out using ciftify_recon_all command that takes recon_all FreeSurfer 6.0 (https://surfer.nmr.mgh.harvard.edu) outputs and generate CIFTI file for structural measures (e.g., cortical thickness) from the surface. The distortion corrected dMRI images are registered to their own structural T1 images by FMRIB Software Library's (FSL 5.0) FLIRT [54]. First rigid alignment is performed followed by the boundary-based registration by supplying WM segmentation obtained from FreeSurfer as an input argument. For fMRI processing, preprocessed first level images are co-registered to their own structural T1 image using SPM12. Conversion tools provided in ciftify toolbox are used to put preprocessed dMRI data and fMRI data into grayordinates in CIFTI format for further analysis. To project diffusion measures from volume onto the cortical surfaces, a ribbon mapping method is used, in which the volumetric measures are collected along the GM ribbon defined by white and pial surfaces, as described in [16]. Unfortunately, there are no T2 weighted images available in our custom dataset. Thus, myelin-style volume to surface mapping is infeasible for our diffusion analysis since myelin maps are unavailable. The grayordinates are based on the low-resolution standard mesh (with ~32 k vertices in each hemisphere) at 2 mm resolution with a total of ~64 k cortical vertices for both hemispheres obtained with the default settings. The low-resolution standard mesh is the suggested template that is appropriate for cross-subject analysis of low-resolution data like dMRI or fMRI.

Processing time comparison between N-GSBSS and SBR using FreeSurfer are reported in Table 1. We used a single thread (Intel Xeon CPU E5-2630 v4 @ 2.20GHz and 32 GB of RAM) on an Ubuntu 16.04 LTS Linux Workstation.

2.7. Simulation study setup

The spherical masks with a radius of 3, 4, and 5 mm were created in template space and transferred back to subject space via the inverse transformation from ANTs SyN [55] registration for each subject. This range was chosen since the cortex is around < 5 mm thick and because capturing the ROIs with different radii could reflect the differences in accounting for partial volume effects in the GM and WM border regions. The location was chosen to contain cortical folding that is variable across multiple subjects to account for partial volume effects when performing cross subject studies.

The GM probability maps for the 30 subjects were randomly divided into two groups, G1 and G2, with 15 subjects in each group. The GM probability data in G2 were then modified in the subject space to simulate percentage change of intensity values in intervals of 10% in the corresponding mask regions. A total of 27 combinations (3 masks and 9 different scalings) were considered for evaluation.

With 0% change, the images in G2 were the same as original images. Thus, we considered the difference between the groups as a baseline. We excluded 100% change of the region of interest in G2, which is completely reduced to zero. With 50% change, the intensity values were half of the original values in ROIs from G2 images.

GM probability data from each of the 27 combinations in G2 were then processed through N-GSBSS to place all the data on the target surface for cross-sectional analysis. GM probability data were also evaluated for VBR, SBR and ciftify for comparison with the same parameter/experimental settings, including 2 mm Gaussian kernel smoothing. Non-parametric permutation tests were then performed between G1 and G2 for all combinations using FSL's PALM [53] package with 5000 iterations.

To assess the sensitivity of the approaches, we examined the ratio of maximum t-statistic ("t-stat ratio"), which was defined as the amount of scaling with respect to the baseline. To have a single metric with comparable result across all the methods, we reported the ratio with respect to baseline. Baseline is where we performed second level analysis for group differences across the 2 groups where no changes are applied to original GM probability maps.

Table 1
Processing time comparison for SBR, ciftify and N-GSBSS based approaches. In SBR, a spherical mapping was conducted for each hemisphere followed by spherical registration. Details of time taken for each step are provided in the processing details column.

Pipeline	Processing steps details	Total time
SBR	Per hemisphere: FSRUNTIME@ mris_sphere 1.48 h, 1 thread FSRUNTIME@ mris_register 0.80 h, 1 thread	~273.6 min
Ciftify	ReconAll (mris_sphere and mris_register): 4.71 h h, 1 thread Ciftify: 1 h 5 min, 1 thread	~345 min
N-GSBSS	ANTs volume registration: ~2.12 min, 1 thread DSM surface registration: ~1.49 min, 1 thread	~4 min

3. Results

In this section, we present the results of all the N-GSBSS analysis as follows: 1) Qualitative results of mean ODI with and without search in comparison with the ciftify pipeline 2) Application in fMRI to identify active regions in task based working memory. 3) GM simulation results in structural MRI based on varying ROI size and intensity differences.

Mean ODI values across 30 subjects are shown on the target surface (Fig. 4) for N-GSBSS without search, with cortical ODI search and the ciftify pipeline. With cortical ODI search, partial volume effects are addressed reflecting higher ODI across the cortex compared to that of other two approaches.

3.1. Working memory fMRI results

As an application of N-GSBSS in fMRI, working memory data was processed for 30 healthy subjects in cue, probe and delay tasks. We compared significant regions revealed by VBR, SBR, the ciftify pipeline and N-GSBSS methods as shown in Fig. 5. For all these tasks, the overall activation pattern is comparable across different methods. As expected, the significant vertices in VBR are fewer and more scattered than the cortical surface-based approaches of SBR, ciftify and N-GSBSS.

Quantitative representation of the number of significant vertices with $p < 0.05$ for all the three tasks are shown in Fig. 6. Note that N-GSBSS has a higher number of significant vertices in all the tasks than VBR, SBR and ciftify pipeline results. The ciftify pipeline results are comparable to that of N-GSBSS more than VBR or SBR approaches. Applying cortical ODI search further improved the activation percentage in N-GSBSS.

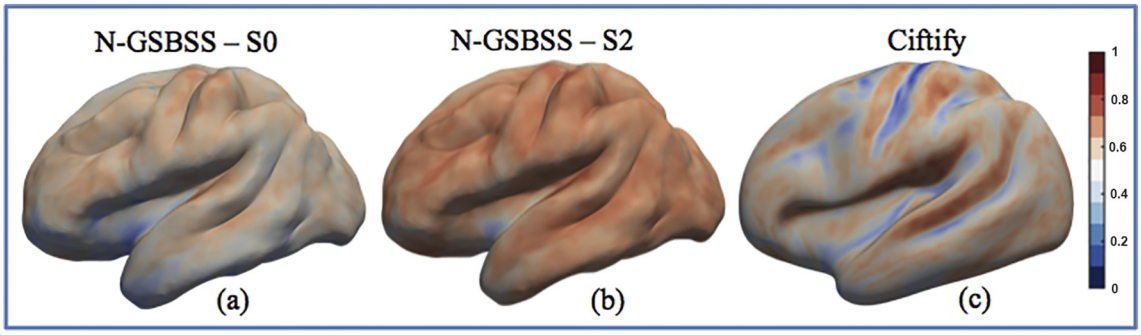

Fig. 4. Mean ODI across 28 healthy subjects using (a) N-GSBSS – S0 with no search (a) N-GSBSS - S2 including ODI search of 2 mm (c) ciftify pipeline. The ciftify results are based on the "gray ordinates" with 64 thousand vertices (the suggested tessellation) on both left and right hemispheres while the target surface template used in N-GSBSS has about 261 thousand vertices.

3.2. Simulation study in structural MRI with changes in regions of interest

Here, we evaluate N-GSBSS with respect to VBR, SBR and ciftify pipeline techniques in identifying sensitivity and specificity of changes in GM voxels located in spherical ROIs of 3, 4, and 5 mm radius located in a region of the frontal cortex. Fig. 7 illustrates spheres with a radius of 5 and 3 mm.

Quantitative results in Fig. 8 show the t-statistics ratio for varying ROI sizes of 3 mm, 4 mm, and 5 mm, and percentage change in the GM probability values from 10% to 90% in the intervals of 10%. T-stat ratio is the maximum t-statistic for each scenario with respect to the baseline to reflect how much it was scaled with induced changes in the region of interest. The baseline is chosen to be the differences between the 2 groups in the current experiment. For VBR, to capture the intensity difference between groups, the probability change must be at least 40% with 5 mm spherical ROI, 50% for 4 mm, and 60% for 3 mm ROI. SBR results showed sensitivity for 20% change with 5 mm ROI. However little difference is observed between baseline and 4 mm ROI from 40% and no difference was captured with 3 mm ROI. N-GSBSS results are much more sensitive starting at 10% with 5 mm ROI, 20% with 4 mm and 30% for 3 mm spherical ROI. N-GSBSS also showed higher maximum t-statistics than SBR. With higher intensity differences starting at 70%, VBR results have higher t-statistic ratio than that of N-GSBSS. In all other cases N-GSBSS has higher maximum t-statistic ratio and better sensitivity.

4. Discussion

Herein, we describe an approach for carrying out multi-modal spatial statistics in low resolution images by taking advantage of high resolution T1 weighted images that are acquired as part of the scan protocol. This approach favorably compares with traditional volume based analyses and with respect to the FreeSurfer surface registration approach along with the ciftify pipeline. Our approach offers an advantage over VBM by achieving improved cortical alignment in agreement with other surface-based registration techniques [25,28–33]. Moreover, in comparison with FreeSurfer, SBR, and ciftify pipelines, the N-GSBSS approach showed an improvement in sensitivity. It suggests that the initial alignment obtained by non-rigid deformation from the T1 image provides a deformed cortical shape that makes surface registration much easier. Consequently, this improves the statistical power compared to existing approaches.

The key aspect of this work is the addition of NODDI based search, which ensures that metrics from low-resolution images are retrieved from highly probable GM. It is achieved by making use of the ODI measure from NODDI which is known to be higher in GM compared to that of WM [43]. Thus by searching for maximum ODI, alignment issues after co-registration or PVE effects from underlying voxels is addressed. The patterns of mean ODI are comparable between these methods with higher values along the gyral regions. The overall mean ODI values in ciftify approach appear to be less than that of the GSBSS approach with or without search (Fig. 4). Lower values could be due to the partial

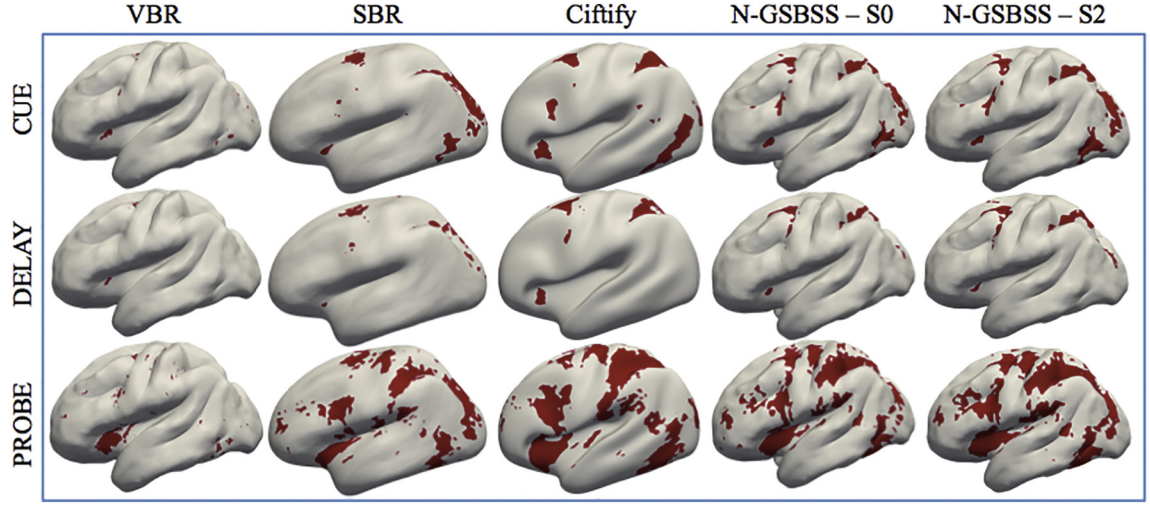

Fig. 5. Working memory fMRI data were processed for 28 healthy controls and results are reported for (a) correct cue, (b) correct delay (c) correct probe tasks with 2 mm smoothing for VBR, SBR, ciftify, N-GSBSS-S0 with no search and N-GSBSS-S2 with 2 mm search methods. Significant p-values after FWE correction based on non-parametric randomize one sample *t*-test with 10,000 iterations are reported. $P_{fwe} < 0.05$ are highlighted in red. (For interpretation of the references to color in this figure legend, the reader is referred to the web version of this article.)

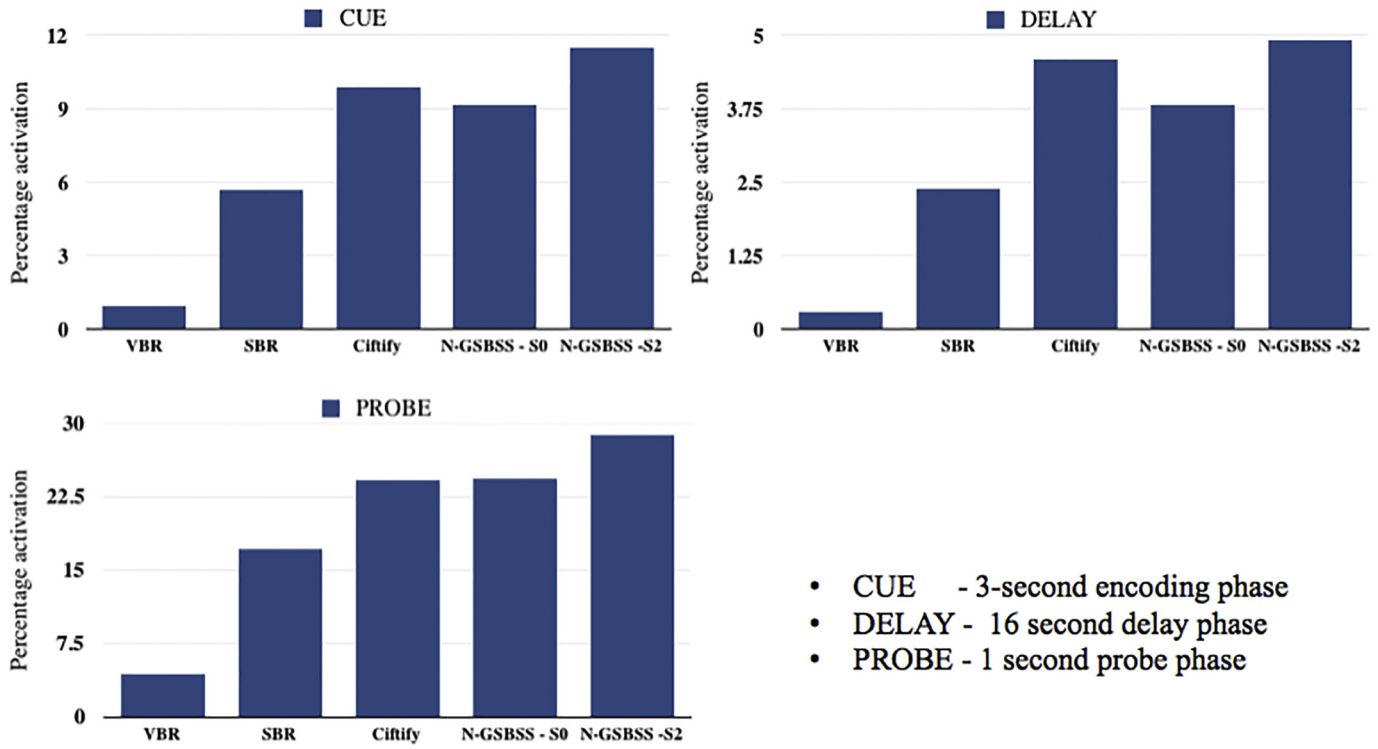

Fig. 6. Percentage activation of working memory fMRI data were processed for 28 healthy controls and results are reported for (a) correct cue, (b) correct delay (c) correct probe tasks with 2 mm smoothing for VBR, SBR, ciftify, N-GSBSS-S0 with no search and N-GSBSS-S2 with 2 mm search methods. The number of significant vertices, with p-values < 0.05 after FWE correction based on nonparametric randomize one sample *t*-test with 10,000 iterations, is divided by total number of vertices and the percentage is reported.

volume effects arising from thinner cortex regions as acknowledged in Fukutomi et al.'s paper [56] indicating the possibility of residual PVE effects in the regions of thinner cortex. When compared to mean ODI values reported in Fukutomi et al.'s paper, the results indicated in our study have higher ODI values across all the methods. Possible reason for this deviation could be due to the number of differences between the two datasets like demographics, data acquisition, and processing. Also we followed the original NODDI model which has empirical settings as mentioned below where $d_{||} = 1.7 \times 10^{-3}\,mm^2/s$, to be representative of both white and gray matter on two-shell data (b = 1000/2000 s/mm^2), while in Fukutomi et al., paper [56] $d_{||}$ is calculated to be 1.1 (0.1) $\times 10^{-3}\,mm^2/s$ for gray matter from an empirically chosen range and the results reported are based on three-shell data (b = 1000/2000/3000 s/mm^2). While the preliminary normal search proposed based on higher ODI seems to improve sensitivity for the changes occurring in pure gray matter, these results may have to be carefully reviewed if a regional variation is essential for the study of interest.

As we are interested in low resolution with dMRI acquired at 2.5 mm resolution and fMRI at 3 mm resolution, we are assuming that after co-registration to T1, the underlying data is roughly aligned at voxel level. Thus we utilize the search map obtained from diffusion modality to apply to fMRI for getting the data based on enclosing voxel approach. The reported fMRI t-statistics suggest an improvement in sensitivity with N-GSBSS. While there is no ground truth for validating the implication of the higher activation, since the contrast maps are relative to that of the un-modeled baseline across 30 subjects, the activation could indicate that the proposed method could be highly sensitive to capture underlying variations that are indirectly contributing to the activations instead of capturing the false positives.

The simulation study is set up to perform sensitivity or specificity check for N-GSBSS to the underlying changes in tissue microstructure. As we are interested in performing analysis in psychiatric applications including schizophrenia [57,58] that are known to have changes in prefrontal region, the ROI is chosen from this region. The GM

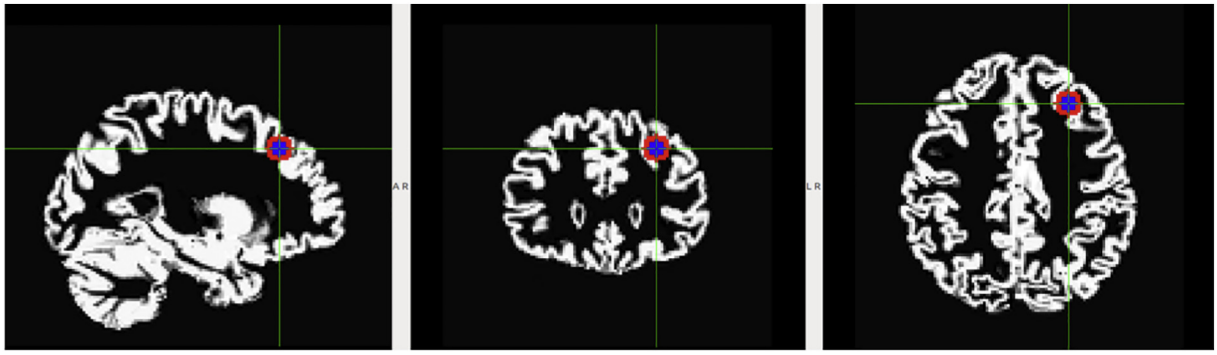

Fig. 7. The gray matter probability map shows the simulated effect as an overlay mask of 5 mm (red) and 3 mm (dark blue) spheres. (For interpretation of the references to color in this figure legend, the reader is referred to the web version of this article.)

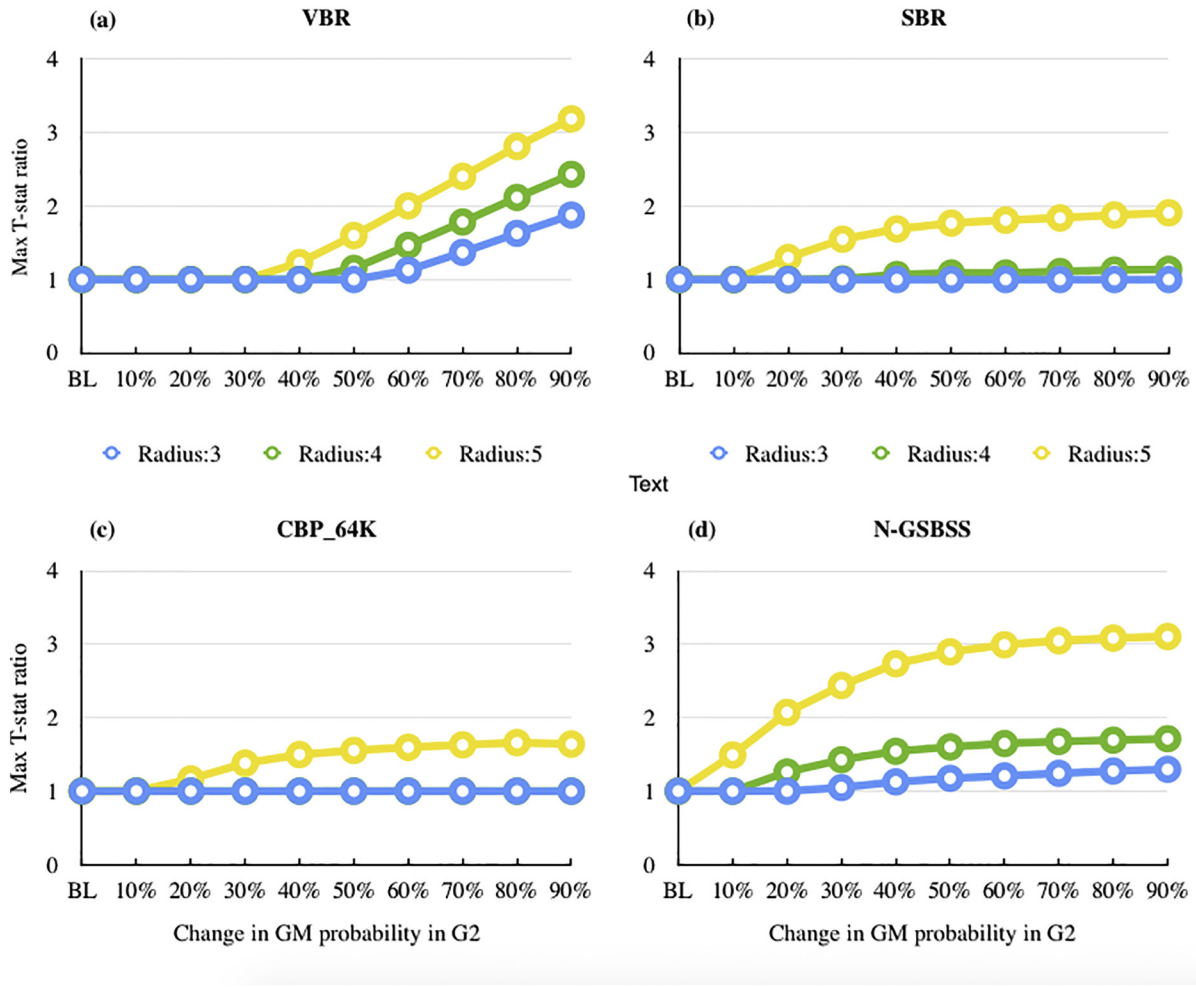

Fig. 8. Quantitative results for statistical group differences over the change in ROI size from 3 to 5 mm and percentage change from 10% to 90%. (a) Results from VBR analysis. (b) Results from FreeSurfer registration analysis. (c) Results from ciftify pipeline with default gray ordinates. (d) Results from GSBSS based analysis. Y-axis indicates maximum t-statistic ratio with respect to baseline. X-axis indicates the percentage change of GM probability in G2 with respect to original GM probability images in G2.

probability map is chosen as the parameter of interest and the intensity changes are simulated within an ROI region. Compared to the baseline methods, N-GSBSS showed superior sensitivity to the underlying changes in both intensity and the size of the ROI as shown in Fig. 8. While volume-based analysis was not able to detect any significant differences between groups for at least up to 50% change in the GM probability values, N-GSBSS was able to capture differences starting from 10% change with ROI size of 5 mm, 20% for 4 mm and 30% for 3 mm. The low performance of VBM could be potentially due to partial volume effects prevalent in the volume-based approach even after applying the GM mask to limit the analysis to highly probable GM regions.

In the simulation study, SBR analysis showed a similar pattern as N-GSBSS. However, the sensitivity of this approach is not as high as N-GSBSS. Differences between the methods are likely due to different registration approaches since both of them used the same surface to obtain corresponding GM probability values from the volume image. The ciftify pipeline results are similar to those of SBR, which is expected since the ciftify pipeline uses FreeSurfer registration. The subtle difference between ciftify and SBR are observed likely due to the different surface reconstruction in each of these pipelines. For a fair comparison, we used the ciftify pipeline with default parameters to the extent possible. For example, the analysis results in the ciftify pipeline are based on the "gray ordinates" with 64 k vertices (the suggested tessellation for cross subject analysis of low resolution data) on both left and right hemispheres. This surface tessellation differs from that of the target central surface used in SBR and N-GSBSS analysis (about 261 k vertices for both hemispheres). This could have contributed to the lower sensitivity of ciftify pipeline in this simulation study due to the limited ability to capture smaller ROI regions with less number of vertices. The higher sensitivity of N-GSBSS to capture GM probability percentage changes as low as 10% for 5 mm ROI and 40% for smaller ROI of 3 mm ROI could indicate that it is able to capture more number of highly probable vertices accurately. In future, additional validations could be performed to evaluate the performance for different resolutions and also at different ROI locations.

5. Conclusion

Overall significant regions captured by N-GSBSS agree with those of VBR, SBR, and ciftify pipelines across different modalities while achieving high spatial specificity. It is highly likely that the volumetric transformation already deformed cortical surfaces into similar shapes (geometry) before the surface registration, which results in better shape correspondence by reducing the local anatomical ambiguity in the surface registration. N-GSBSS possesses high flexibility that allows any registration method as well as multiple modalities. We expect that such a feature can be generally extended to various modalities in general neuroimaging studies.

An operational virtual machine and source code for N-GSBSS are posted in a Docker image: (https://github.com/MASILab/N-GSBSS/).

Acknowledgements

This work was conducted in part using the resources of the Advanced Computing Center for Research and Education at Vanderbilt University, Nashville, TN. This project was supported in part by the National Center for Research Resources, Grant UL1 RR024975-01, and is now at the National Center for Advancing Translational Sciences, Grant 2 UL1 TR000445-06 and NIH R01EB017230 & R01MH102266. The content is solely the responsibility of the authors and does not necessarily represent the official views of the NIH.

Appendix A. Supplementary data

Supplementary data to this article can be found online at https://doi.org/10.1016/j.mri.2019.05.016.

References

[1] Woodward ND. Thalamocortical functional connectivity, cognitive impairment, and cognitive remediation in schizophrenia. Biol Psychiatry 2017;2(4):307–9.
[2] Gennatas ED, Avants BB, Wolf DH, Satterthwaite TD, Ruparel K, Ciric R, et al. Age-related effects and sex differences in gray matter density, volume, mass, and cortical thickness from childhood to young adulthood. J Neurosci 2017;37(20):5065–73.
[3] Gold AL, Steuber ER, White LK, Pacheco J, Sachs JF, Pagliaccio D, ... Pine DS. Cortical thickness and subcortical gray matter volume in pediatric anxiety disorders. Neuropsychopharmacology 2017;42(12):2423.
[4] Gong NJ, Chan CC, Leung LM, Wong CS, Dibb R, Liu C. Differential microstructural and morphological abnormalities in mild cognitive impairment and Alzheimer's disease: evidence from cortical and deep gray matter. Hum Brain Mapp 2017;38(5):2495–508.
[5] Korponay C, Dentico D, Kral T, Ly M, Kruis A, Goldman R, ... Davidson RJ. Neurobiological correlates of impulsivity in healthy adults: lower prefrontal gray matter volume and spontaneous eye-blink rate but greater resting-state functional connectivity in basal ganglia-thalamo-cortical circuitry. NeuroImage 2017;157:288–96.
[6] Tóth E, Szabó N, Csete G, Király A, Faragó P, Spisák T, et al. Gray matter atrophy is primarily related to demyelination of lesions in multiple sclerosis: a diffusion tensor imaging MRI study. Front Neuroanat 2017;11.
[7] Calhoun VD, Adali T, Giuliani NR, Pekar JJ, Kiehl KA, Pearlson GD. Method for multimodal analysis of independent source differences in schizophrenia: combining gray matter structural and auditory oddball functional data. Hum Brain Mapp 2006;27(1):47–62.
[8] Shen D, Cui L, Fang J, Cui B, Li D, Tai H. Voxel-wise meta-analysis of gray matter changes in amyotrophic lateral sclerosis. Front Aging Neurosci 2016;8:64.
[9] Nazeri A, Mulsant BH, Rajji TK, Levesque ML, Pipitone J, Stefanik L, et al. Gray matter neuritic microstructure deficits in schizophrenia and bipolar disorder. Biol Psychiatry 2017;82(10):726–36.
[10] Ekman CJ, Petrovic P, Johansson AG, Sellgren C, Ingvar M, Landén M. A history of psychosis in bipolar disorder is associated with gray matter volume reduction. Schizophr Bull 2016;43(1):99–107.
[11] Nazeri A, Chakravarty MM, Rotenberg DJ, Rajji TK, Rathi Y, Michailovich OV, et al. Functional consequences of neurite orientation dispersion and density in humans across the adult lifespan. J Neurosci 2015;35(4):1753–62.
[12] Carmona S, Vilarroya O, Bielsa A, Tremols V, Soliva JC, Rovira M, et al. Global and regional gray matter reductions in ADHD: a voxel-based morphometric study. Neurosci Lett 2005;389(2):88–93.
[13] Thompson PM, Hayashi KM, de Zubicaray G, Janke AL, Rose SE, Semple J, et al. Dynamics of gray matter loss in Alzheimer's disease. J Neurosci 2003;23(3):994–1005.
[14] Von Economo C. The cytoarchitectonics of the human cerebral cortex. H. Milford Oxford University Press; 1929.
[15] Von Economo C, Koskinas G. The cytoarchitectonics of the adult human cortex. Vienna and Berlin: Julius Springer Verlag; 1925.
[16] Glasser MF, Smith SM, Marcus DS, Andersson JL, Auerbach EJ, Behrens TE, et al. The human connectome Project's neuroimaging approach. Nat Neurosci 2016;19(9):1175–87.
[17] Jones DK, Cercignani M. Twenty-five pitfalls in the analysis of diffusion MRI data. NMR Biomed 2010;23(7):803–20.
[18] Smith SM, Jenkinson M, Johansen-Berg H, Rueckert D, Nichols TE, Mackay CE, et al. Tract-based spatial statistics: voxelwise analysis of multi-subject diffusion data. Neuroimage 2006;31(4):1487–505.
[19] Bodini B, Khaleeli Z, Cercignani M, Miller DH, Thompson AJ, Ciccarelli O. Exploring the relationship between white matter and gray matter damage in early primary progressive multiple sclerosis: an in vivo study with TBSS and VBM. Hum Brain Mapp 2009;30(9):2852–61.
[20] Westlye LT, Walhovd KB, Dale AM, Bjørnerud A, Due-Tønnessen P, Engvig A, et al. Life-span changes of the human brain white matter: diffusion tensor imaging (DTI) and volumetry. Cereb Cortex 2009;20(9):2055–68.
[21] Olson EA, Cui J, Fukunaga R, Nickerson LD, Rauch SL, Rosso IM. Disruption of white matter structural integrity and connectivity in posttraumatic stress disorder: a TBSS and tractography study. Depression and anxiety 2017;34(5):437–45.
[22] Bells S, Lefebvre J, Prescott SA, Dockstader C, Bouffet E, Skocic J, et al. Changes in white matter microstructure impact cognition by disrupting the ability of neural assemblies to synchronize. J Neurosci 2017;37(34):8227–38.
[23] Goodrich-Hunsaker NJ, Abildskov TJ, Black G, Bigler ED, Cohen DM, Mihalov LK, et al. Age-and sex-related effects in children with mild traumatic brain injury on diffusion magnetic resonance imaging properties: a comparison of voxelwise and tractography methods. J Neurosci Res 2018;96(4):626–41.
[24] Gray matter surface based spatial statistics (GS-BSS) in diffusion microstructure. In: Parvathaneni P, Rogers BP, Huo Y, Schilling KG, Hainline AE, Anderson AW, editors. International conference on medical image computing and computer-assisted intervention. Springer; 2017.
[25] Jo HJ, Lee JM, Kim JH, Shin YW, Kim IY, Kwon JS, et al. Spatial accuracy of fMRI activation influenced by volume- and surface-based spatial smoothing techniques. Neuroimage 2007;34(2):550–64.
[26] Bookstein FL. "Voxel-based morphometry" should not be used with imperfectly registered images. Neuroimage 2001;14(6):1454–62.
[27] Crum WR, Griffin LD, Hill DL, Hawkes DJ. Zen and the art of medical image registration: correspondence, homology, and quality. Neuroimage 2003;20(3):1425–37.
[28] Oosterhof NN, Wiestler T, Downing PE, Diedrichsen J. A comparison of volume-based and surface-based multi-voxel pattern analysis. Neuroimage 2011;56(2):593–600.
[29] Dale AM, Fischl B, Sereno MI. Cortical surface-based analysis. I. Segmentation and surface reconstruction. Neuroimage 1999;9(2):179–94.
[30] Fischl B, Sereno MI, Dale AM. Cortical surface-based analysis. II: inflation, flattening, and a surface-based coordinate system. Neuroimage 1999;9(2):195–207.
[31] Wandell BA, Chial S, Backus BT. Visualization and measurement of the cortical surface. J Cogn Neurosci 2000;12(5):739–52.
[32] Van Essen DC, Drury HA, Dickson J, Harwell J, Hanlon D, Anderson CH. An integrated software suite for surface-based analyses of cerebral cortex. J Am Med Inform Assoc 2001;8(5):443–59.
[33] Yeo BT, Sabuncu MR, Vercauteren T, Ayache N, Fischl B, Golland P. Spherical demons: fast diffeomorphic landmark-free surface registration. IEEE Trans Med Imaging 2010;29(3):650–68.
[34] Van Essen DC. A population-average, landmark-and surface-based (PALS) atlas of human cerebral cortex. Neuroimage 2005;28(3):635–62.
[35] Fischl B, Sereno MI, Tootell RB, Dale AM. High-resolution intersubject averaging and a coordinate system for the cortical surface. Hum Brain Mapp 1999;8(4):272–84.
[36] Van Essen D, Drury H. Structural and functional analyses of human cerebral cortex using a surface-based atlas. J Neurosci 1997;17(18):7079–102.
[37] Van Essen David C, Smith Stephen M, Barch Deanna M, EJ Behrens Timothy, Yacoub Essa, Ugurbil Kamil, HCP Consortium Wu-Minn. The WU-Minn human connectome project: an overview. Neuroimage 2013;80:62–79.
[38] Glasser MF, Sotiropoulos SN, Wilson JA, Coalson TS, Fischl B, Andersson JL, et al. The minimal preprocessing pipelines for the human connectome project. Neuroimage 2013;80:105–24.
[39] Robinson EC, Jbabdi S, Glasser MF, Andersson J, Burgess GC, Harms MP, et al. MSM: a new flexible framework for multimodal surface matching. Neuroimage 2014;100:414–26.
[40] Glasser MF, Coalson TS, Robinson EC, Hacker CD, Harwell J, Yacoub E, et al. A multi-modal parcellation of human cerebral cortex. Nature 2016;536(7615):171–8.
[41] Robinson EC, Garcia K, Glasser MF, Chen Z, Coalson TS, Makropoulos A, et al. Multimodal surface matching with higher-order smoothness constraints. NeuroImage 2018;167:453–65.
[42] Dickie EW, Anticevic A, Smith DE, Coalson TS, Manogaran M, Calarco N, et al. Ciftify: a framework for surface-based analysis of legacy MR acquisitions. bio Rxiv 2018:484428.
[43] Zhang H, Schneider T, Wheeler-Kingshott CA, Alexander DC. NODDI: practical in vivo neurite orientation dispersion and density imaging of the human brain. Neuroimage 2012;61(4):1000–16.
[44] Ashburner J. A fast diffeomorphic image registration algorithm. Neuroimage 2007;38(1):95–113.
[45] Lombaert H, Sporring J, Siddiqi K. Diffeomorphic spectral matching of cortical surfaces. Inf Process Med Imaging 2013;23:376–89.
[46] Asman AJ, Landman BA. Non-local statistical label fusion for multi-atlas segmentation. Med Image Anal 2013;17(2):194–208.
[47] Open labels: online feedback for a public resource of manually labeled brain images. In: Klein A, Dal Canton T, Ghosh SS, Landman B, Lee J, Worth A, editors. 16th annual meeting for the Organization of Human Brain Mapping. 2010.
[48] Huo Y, Carass A, Resnick SM, Pham DL, Prince JL, Landman BA. Combining multi-atlas segmentation with brain surface estimation. Proceedings of SPIE–the International Society for Optical Engineering. NIH Public Access; 2016.
[49] Andersson JLR, Sotiropoulos SN. An integrated approach to correction for off-resonance effects and subject movement in diffusion MR imaging. Neuroimage 2016;125:1063–78.
[50] Smith SM, Jenkinson M, Woolrich MW, Beckmann CF, Behrens TE, Johansen-Berg H, et al. Advances in functional and structural MR image analysis and implementation as FSL. Neuroimage 2004;23(Suppl. 1):S208–19.
[51] Smith SM. Fast robust automated brain extraction. Hum Brain Mapp 2002;17(3):143–55.
[52] Ashburner J, Friston KJ. Voxel-based morphometry–the methods. Neuroimage 2000;11(6 Pt 1):805–21.
[53] Winkler AM, Ridgway GR, Webster MA, Smith SM, Nichols TE. Permutation inference for the general linear model. Neuroimage 2014;92:381–97.

[54] Jenkinson M, Bannister P, Brady M, Smith S. Improved optimization for the robust and accurate linear registration and motion correction of brain images. Neuroimage 2002;17(2):825–41.
[55] Avants BB, Epstein CL, Grossman M, Gee JC. Symmetric diffeomorphic image registration with cross-correlation: evaluating automated labeling of elderly and neurodegenerative brain. Med Image Anal 2008;12(1):26–41.
[56] Fukutomi H, Glasser MF, Zhang H, Autio JA, Coalson TS, Okada T, et al. Neurite imaging reveals microstructural variations in human cerebral cortical gray matter. Neuroimage 2018;182:488–99.
[57] Sheffield J, Parvatheni P, Rogers B, Landman B, Woodward N. T222. functional brain activation and grey matter integrity in psychosis: a combined functional magnetic resonance and neurite orientation distribution and density imaging study. Biol Psychiatry 2018;83(9):S214-S5.
[58] Neurite orientation dispersion and density imaging (NODDI) of the prefrontal cortex in psychosis. In: Woodward ND, Parvatheni P, Rogers B, Damon S, Landman B, editors. Biological psychiatry. 360 Park Ave South, New York, Ny 10010–1710 USA: Elsevier Science Inc; 2017.
[59] Glasser Matthew F, Van Essen David C. Mapping human cortical areas in vivo based on myelin content as revealed by T1-and T2-weighted MRI. Journal of Neuroscience 2011;31(32):11597–616.